Received: 13 October 2019 | Revised: 15 June 2020 | Accepted: 16 June 2020

DOI: 10.1002/ese3.781

RESEARCH ARTICLE

Energy Science & Engineering
Open Access

Daylight luminescence system for silicon solar panels based on a bias switching method

Miguel Guada[1] | **Ángel Moretón**[1] | **Sofía Rodríguez-Conde**[1,2] | **Luis Alberto Sánchez**[1] | **Mario Martínez**[2] | **Miguel Ángel González**[1] | **Juan Jiménez**[1] | **Leonardo Pérez**[2] | **Vicente Parra**[2] | **Oscar Martínez**[1]

[1]GdS-Optronlab Group, Universidad de Valladolid, Edificio LUCIA, Valladolid, Spain

[2]Enertis Solar S.L., Madrid, Spain

Correspondence
Óscar Martínez, GdS-Optronlab Group, Universidad de Valladolid. Paseo de Belén 19, Edificio LUCIA, Campus Miguel Delibes, 47011 Valladolid, Spain.
Email: oscar@fmc.uva.es

Vicente Parra, Enertis Solar, S.L., Av. Bruselas 31, 28108 Madrid, Spain.
Email: vicente.parra@enertis.es

Abstract

Among the many characterization techniques for solar panel testing, two, electroluminescence (EL) and photoluminescence (PL), can provide useful visual information about the presence of different types of cell defects. EL is performed outdoors by night in commercial solar plants due to the very weak luminescence emission compared to sunlight. PL faces the added difficulty of needing to find a large-area homogeneous light source to excite the modules. Since nighttime work poses many drawbacks and risks, a daylight outdoor EL/PL system would be useful for offering safe inspection of solar plants. We present daylight luminescence techniques based on a bias switching method, in which a pulsed luminescence signal is obtained by alternating the polarization state of the solar panels, synchronizing it with the luminescence image detection by an InGaAs camera. Fast switching and selecting an optimized exposure time are key to achieving high-quality images. The daylight luminescence method described herein allows both EL and PL luminescence images to be obtained, even under high solar irradiance conditions.

KEYWORDS

cell defects, daylight, electroluminescence, photoluminescence, solar panels

1 | INTRODUCTION

Luminescence techniques, both electroluminescence (EL) and photoluminescence (PL), are becoming powerful tools for inspecting solar cells and photovoltaic modules,[1-7] based on the reciprocity relation between photovoltaic quantum efficiency and luminescence emission.[8,9] EL consists of luminescence emission by solar cells under forward bias,[10] thereby spatially resolving defects that affect the performance and/or durability of the modules, such as cracks, heterogeneous cell activity, failed soldering, grid defects, and dark areas in cells associated with dislocation clusters.[11-18] In contrast, PL consists of luminescence emission under excitation with light.[19-28] The difficulty involved in obtaining a uniform large-area light excitation source over the module surface has prevented it from being applied to module inspection. This problem was circumvented by using the sun as the excitation source, without having to resort to an artificial light source, for example, a laser.[19,29] PL emission depends on the quality of the material, its defects, for example, dislocations, precipitates, and cracks,

surface passivation, and effective excitation intensity, while EL also reveals genuine cell defects such as contact defects, shunts, soldering defects, and local resistance changes. The two techniques can therefore provide complementary information about cell and module failures.

Luminescence inspection of silicon modules, both monocrystalline and multicrystalline, is usually performed with high-sensitive low-noise silicon charge-coupled devices (CCD) and CMOS cameras,[30,31] which also offer high resolution. It can be also carried out with stock consumer Si CCD cameras.[32] However, the spectral response of this type of sensor is not the ideal one for capturing the Si emission spectrum. Si-based cameras are only sensitive to the high-energy tail of the intrinsic emission of Si, the peak wavelength of which is ~1100 nm, out of the sensitive spectral window of the camera ($\lambda < 1050$ nm), while they are sensitive to most of the solar irradiance spectrum (Figure 1). Therefore, luminescence imaging of solar modules with Si-based cameras must be carried out in a dark environment so as to avoid background light (ambient noise from the sun or other light sources). These conditions are sufficient when the images are acquired in a laboratory environment free of background light. However, if inspections are carried out at the solar plant, measurements must be performed in PV mobile laboratories[33] or directly outdoors on the installed modules.[4,34] The first option involves dismantling the modules from the plant and placing them into the mobile laboratory. Handling the modules increases the risk of producing microcracks,[35,36] while dismantling the modules and transporting them to the laboratory are time-consuming and costly, and cannot be extended to a large number of modules. Acquiring the outdoor luminescence images directly on the installed modules thus appears to be the best option if the background light is suppressed. One option consists of carrying out the measurements by night when the background light does not blind the luminescence emission. However, nighttime measurements involve several operational and safety issues, such as working under harsh environmental conditions (low temperatures, etc), the use of light towers, and the complexity of motion across the plant during the night to polarize the modules. As a result, nighttime EL is difficult to implement as a routine tool for inspecting the high number of modules that make up a utility-scale solar plant.

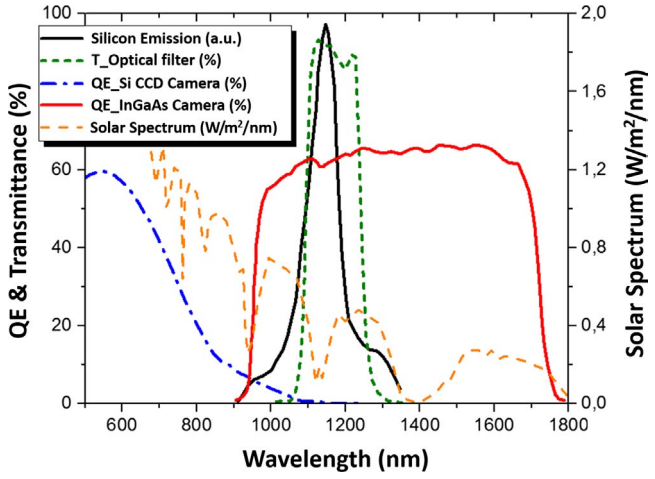

FIGURE 1 Quantum efficiency (QE) of Si and InGaAs detectors. The luminescence spectrum of Si and the transmittance (T) of the band-pass optical filter used are also shown. Solar spectrum irradiance at AM1.5 is also plotted

In this context, the possibility of achieving outdoor daylight luminescence imaging of the modules emerges as a very attractive option. However, performing daylight luminescence measurements is very challenging, given the need to implement methods which allow the background sun radiation to be suppressed in order to extract the luminescence emitted by the cells.

Different approaches have been proposed to perform outdoor EL imaging (night and day time).[1,4,5,29,34,37-41] With regard to nighttime EL, in 2016 S. Koch and coworkers compared manual ground-level inspections and drone-based aerial surveys, and concluded that the use of a drone, despite certain inconveniences, is the most powerful option for inspecting large solar plants.[4] In order to extend the EL technique to daylight conditions, also in 2016, Adams et al[34] reported what they called the electroluminescence lock-in (ELLI) technique. Basically, the use of a pulsed electrical signal allowed them to detect the EL signal in dark conditions in motion, which was facilitated by the use of an InGaAs camera instead of a Si-based CCD camera. Stoicescu et al[38,39] reported a method to obtain daylight luminescence images of PV panels, based on the polarization of PV panels with an AC-modulated bias correctly synchronized with the camera. Later in 2017, T. Kropp and coworkers presented a novel daylight EL measurement system that uses (for polarization) the power generated by the module itself.[37] GAR Benatto and coworkers have also developed lock-in subtraction EL methods, which can be useful for aerial inspections.[5,40,41] The outdoor acquisition of PL images is also discussed in the literature. Bhoopathy et al[19] proposed a method based on shadowing one cell simultaneously to image acquisition, in order to produce a switching optical generation in the module. Another approach to obtain EL and PL images was proposed by Silverman et al.[29] The idea was to force the module to work in different points of the illuminated I-V curve while imaging the optical generation. Their conclusions show the advantage of EL in terms of image quality, since it contrasts the defects better. What they called open-circuit outdoor PL is a useful characterization method for solar modules.

All of these daylight EL and PL imaging techniques share common principles, although they follow different strategies for filtering the background light, separating EL from PL and optimizing the quality of the images. This article deals with the implementation of a daylight luminescence (EL and PL) tool based on the setup of a switching

procedure which allows ambient light to be filtered effectively (Section 3). This procedure allows high-quality luminescence images of the solar modules, both EL and PL, to be obtained, even under high solar irradiance, with short acquisition times, without dismantling the modules, and with the versatility of being able to be used 24 hours a day. Preliminary results have previously been published.[42] Here, we provide a detailed description of the experimental procedure and data treatment. To the previous published works, we add the ability to acquire consecutive images at two different polarization states with a precise exposure time and with a very high switching frequency. Applying this method involves the use of an InGaAs camera for luminescence acquisition and a solid-state relay controlled by radiofrequency in order to ensure the switching procedure described below.

2 | EXPERIMENTAL

The InGaAs camera used was a 640 × 512 pixels Hamamatsu C12741-03, with 14 bits' resolution. The pixel noise and dark current of this camera are 250 e-rms and 360 000 e-/pixel.s, respectively. The exposure times range from 1 μs to 1 s, which enables acquisition to be adapted to the different lighting conditions that can be found in a solar plant. It has a lightweight (600 g), small size (98 mm × 56 mm × 56 mm), and efficient power consumption (16 W). Moreover, a USB 3.0 interface and LabVIEW drivers allow it to be connected to any computer.

We use a Kowa short-wave infrared (SWIR) optical system with 16 mm focal length for image acquisition. This allows an entire module per image to be viewed with the camera placed 2.5 m away from the module.

Suppressing the ambient light is the critical issue. For this purpose, it is advisable to use a set of appropriate optical filters. The maximum transmittance of the filters should cover the spectral range of the luminescence emission of silicon (Figure 1). In our setup, a SWIR band-pass filter, centered around 1160 nm with a bandwidth of 150 nm and a transmittance close to 90%, is used.

EL measurements require the forward polarization of the module. A power supply giving the necessary voltage output is thus needed. The higher the bias (and hence the forward current), the higher the EL signal. If measurements need to be carried out in accordance with the IEC 60904-13 standard, an equivalent to its short-circuit current for the module polarization is required. According to the most common characteristics of crystalline Si modules, a voltage of about 40 V and a current output of 8-10 A are needed. Depending on the available power supply, just one module or a complete string could be biased. A solid-state relay (Schneider SSP1D412BD) is used to switch the polarization states.

The InGaAs camera (Hamamatsu) was compared with a silicon CCD camera (PCO 1300). The silicon camera has a higher resolution (1392 × 1040 pixels), but a lower bit resolution (12 bits) compared to the InGaAs one. The pixel read noise and dark current of the PCO camera are 6-10 e-rms and 0.05 e-/pixel.s, respectively.

Irradiance was systematically measured in situ using a power meter, in the plane of the modules, just before and after image acquisition.

3 | BIAS SWITCHING METHOD

3.1 | Bias switching method for EL acquisition

As already mentioned, EL measurements using Si sensors need complete darkness. The use of an InGaAs sensor allows for an optimized capture of the Si emission, since it covers the full spectrum emission of Si with high quantum efficiency (Figure 1). In addition, it is blind to visible light such that the detector behaves as a filter for the visible ambient light. However, ambient light also contains IR contributions to which the InGaAs detector is sensitive. Background light is still therefore collected with this detector and must be removed in order to extract the luminescence signal. Daylight luminescence measurements require sophisticated filtering methods to reject the ambient light in order to extract a low-noise luminescence image of the modules.

We considered various filtering alternatives, one of which was a frequency filtering method (lock-in method). This consists of directly biasing the module at a known and controlled frequency, such that the corresponding EL signal emitted by the module is also modulated at that frequency.[39,41,43] By making the Fourier transform for each pixel of the image and by filtering the bias frequency, it is possible to extract the EL signal from each pixel and reconstruct the EL image. This is a very effective method which can be expected to provide satisfactory EL images. However, it is not easy to perform because:

1. modulating the polarization signal at a high frequency is challenging,
2. it is necessary to acquire many images in order to obtain a good sampling rank, and
3. the images need to be filtered after capture, which involves exporting a large volume of data. This proves time-consuming in computing terms and requires computers with a large processing capacity.

These drawbacks led us to implement a simplified approach of this method for acquiring daylight EL images. The procedure consists of subtracting the module/cell images

sequentially recorded under direct polarization (On state) and open circuit (Off state) of the modules. It should be noted that daylight outdoor EL is not exactly equivalent to dark EL, but it is EL under illumination. The light collected by the detector not only consists of the EL emission itself, together with the ambient light (both direct and reflected by the module). The PL emission excited by the sunlight must also be taken into account. In the Off state, the detector collects the ambient light, both reflected and direct, as well as the PL emission. Thus, the background signal (bg), corresponding to the Off state, is subtracted from the signal collected in the On state (background light equivalent to that collected in the Off state plus the EL emission arising from the module, EL + bg).[34] The difference between the images obtained in the two states should provide the EL image. Figure 2 shows the I-V curve under illumination and the scheme of the On and Off states for the EL image acquisition.

Using the bias switching method, images are captured in two different states. The signal level at each pixel of the camera sensor is given by the expression:

$$\text{Pixel Intensity} = A \cdot t_{\text{exp}} \cdot \int \left(\Phi_{\text{EL}}(\lambda) + \Phi_{\text{SUN}}(\lambda)\right) \cdot \text{SR}_{\text{CAM}}(\lambda) \cdot T(\lambda) \cdot \text{d}\lambda \quad (1)$$

where A is a constant, t_{exp} the exposure time of the camera (time during which the sensor is receiving a signal), $\Phi_{\text{EL}}(\lambda)$ the EL signal, $\Phi_{\text{SUN}}(\lambda)$ the total ambient solar irradiance, $\text{SR}_{\text{CAM}}(\lambda)$ the spectral response (sensitivity) of the camera, and $T(\lambda)$ the transmittance of the optical filter (in order to improve the $\Phi_{\text{EL}}(\lambda)/\Phi_{\text{SUN}}(\lambda)$ ratio, see Figure 1).

Exposure time is critical vis-à-vis improving the quality of the images.[44] Under daylight conditions, the intensity of the background light reaching the detector can be very high. As a result, t_{exp} has to be limited in order to avoid saturation of the detector. Figure 3 shows a schematic representation of the variation of pixel intensity under two different levels of ambient light (low and high). The EL signal for the exposure time t_1 in the case of high solar irradiance, $\text{EL}_1^{(\text{high})}$, would be approximately similar to that for low solar irradiance, for which the resulting signal is $\text{EL}_1^{(\text{low})}$. However, the signal-to-noise ratio (SNR), where noise refers to the background light, is higher in the case of low irradiance. In order to improve the quality of the EL image, the exposure time must therefore be optimized with respect to solar irradiance conditions, for which t_2 rather than t_1 should be selected for the case of low irradiance conditions. The horizontal line in the graph of Figure 3 represents the "saturation level," which is the threshold light intensity saturating the InGaAs camera. The selected exposure time should always allow the camera to operate in a safety range below the saturation threshold, given that a slight increase in solar irradiance is sufficient to take the overall light intensity over the saturation threshold of the pixel when working close to such a threshold.

The image subtraction method encounters a limit when the EL signal is too weak compared to the background light (EL + bg ≈ bg). Obviously, this depends on the bg light and the experimental setup, as well as the detector and filters. As a result, in order to ensure better performance, the experimental systems need to be improved by enhancing the EL/bg ratio.

The bias switching method can be significantly improved by acquiring several consecutive On/Off images (cycles).[29,40,45] The final EL image will be obtained by averaging the images extracted from the subtraction of each pair

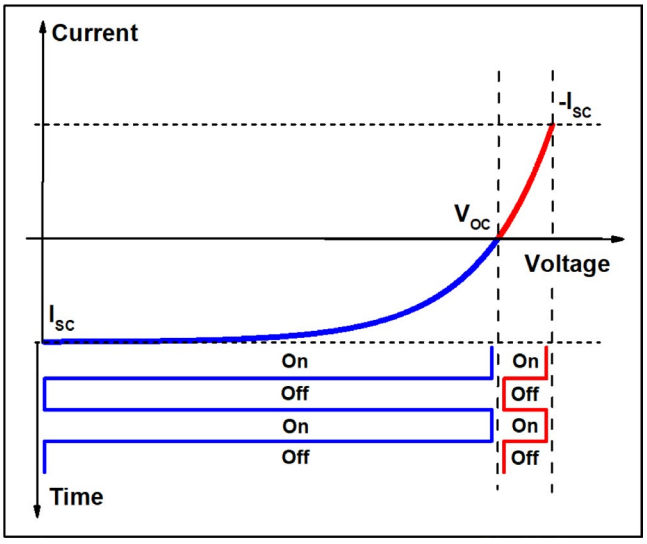

FIGURE 2 Representation, over a daylight solar panel I-V curve, of the two polarization states to obtain EL images (On/Off states, in red color). (On/Off states for PL images are depicted in blue)

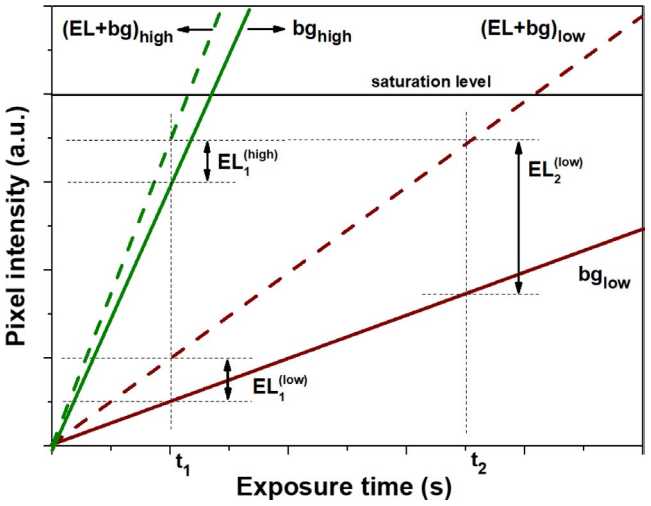

FIGURE 3 Schematic relationship between the intensity of a pixel and the exposure time used, for the cases of high (green lines) and low (brown lines) solar irradiance

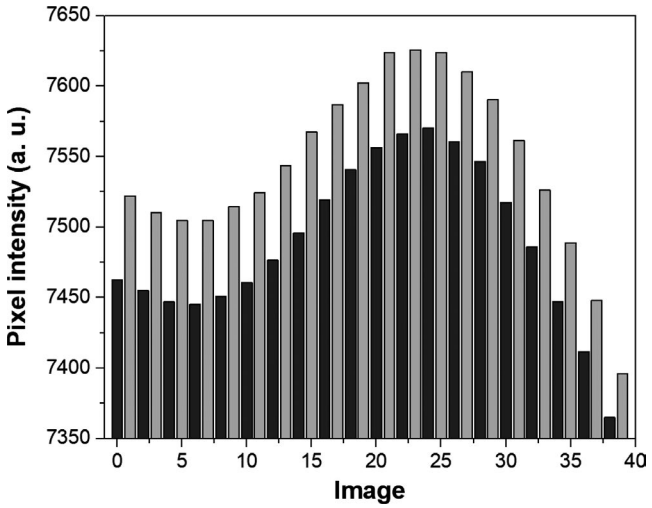

FIGURE 4 Average light levels in all pixels of an image, acquired with 20 On/Off measurement cycles

of On/Off images over a number of cycles. Figure 4 shows the measured signal intensity levels received by the InGaAs detector along a measurement consisting of 20 consecutive Off/On cycles. Here, the height of the bars is given by the average value of all the pixels in an image. The difference between the two intensities is the EL signal. This image illustrates two relevant conclusions: (a) The SNR is very low, ≈0.01, which is the result of the weak EL signal with respect to the background light. Even under such unfavorable conditions, image subtraction allows the EL signal to be extracted. (b) A major fluctuation in ambient sunlight conditions, of the order of the EL signal in this case, can occur in a relatively short time, such as 20 seconds. Consecutive On/Off images, and their average over a number of cycles, allow the ambient light variations which occur during the acquisition process to be corrected. Fast On/Off switching, as well as a short exposure time, permits the temporal fluctuations of the ambient light intensity to be reduced.

It is important to distinguish between the exposure time of the camera (t_{exp}), the total acquisition time (t_{ac}), the processing time used in the subtractions and averages of each block of images (t_p), and the total time for obtaining the final EL image (t_T), which is the sum of all the other times. The total acquisition time (t_{ac}) is the addition of the exposure time, which can be as short as 1 μs for the used camera, plus the processing time of the camera, which for this camera has a fixed value of 16.7 ms. Although t_{exp} can be very short with respect to the processing time, it plays an important role in image acquisition. The processing time used for the subtractions and averages (t_p) of each block of images largely determines the total time (t_T). The processing time depends to a great extent on software design and hardware capabilities.

3.2 | Bias switching method for PL acquisition

We implemented a procedure equivalent to the bias switching used for the EL images in order to extract the daylight PL images. This is not so straightforward in this case because the sunlight excitation source cannot be switched off, as was done for the module polarization in the EL measurements. To achieve the Off and On excitation states in PL measurements, one works with the photovoltaic module in either open circuit (On state) or short circuit (Off state) (see the On and Off states on the I-V curve under illumination in Figure 2). When the photovoltaic module is in open circuit under solar irradiance, the photogenerated electrons and holes remain spatially close, and a significant fraction of them can recombine radiatively, giving the PL signal (On state), which is superposed to the background light. It should be noted that the PL On state is equivalent to the EL Off state. In contrast, when the module is short-circuited, most of the photogenerated electrons and holes are driven away by the induced reverse photovoltage, and only a small population of the electrons and holes recombine, with the subsequent decrease in the PL signal, which allows us to take it as the Off state. The difference between the luminescence signals acquired under each of these measurement conditions should allow the daylight PL image to be extracted. The sequential acquisition of PL images in On and Off states follows the same trends described for acquiring EL images.

Daylight PL evidences certain limitations compared to daylight EL. The main one of these is the need for a threshold solar irradiance level in order to have sufficient excitation to generate a measurable PL signal. This issue is discussed later on.

It is worth noting that EL and PL are complementary with respect to the irradiance conditions. EL images improve under low solar irradiance conditions, while PL measurements need a threshold level of solar irradiance to generate sufficient signal, and improve when solar irradiance increases. For high solar irradiance conditions, EL measurements will present more noise and therefore will demand a high number of On/Off cycles while such conditions can prove to be advantageous for PL measurements. In contrast, under low solar irradiance, PL measurements might not be feasible whereas EL measurements provide excellent results. On the other hand, PL measurements do not need the use of an external DC power supply.

3.3 | Hardware and software for implementing the procedure

Figure 5 shows a scheme of the daylight EL system. In order to have very precise polarization control (On and Off cycles) and to minimize the problems caused by cable interconnections, a home-made radio frequency module controlled by

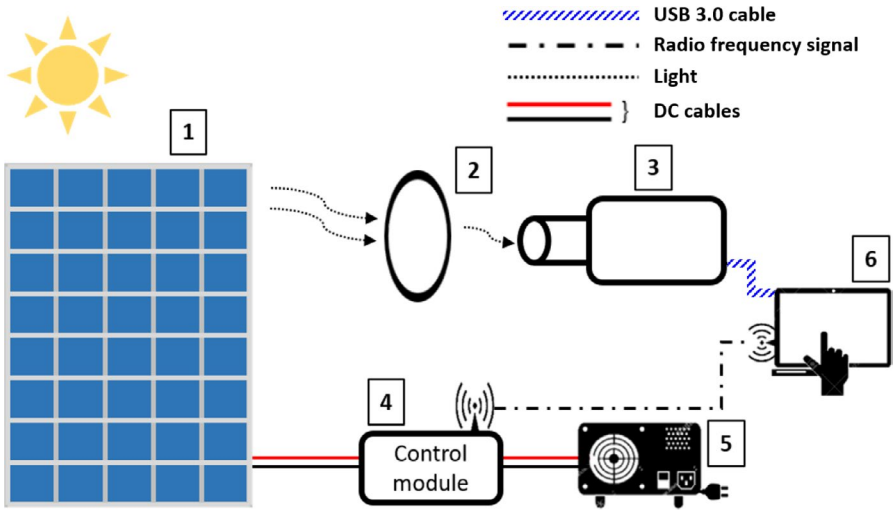

FIGURE 5 Daylight EL system diagram. 1—Solar radiation; 2—band-pass optical filter; 3—InGaAs camera; 4—radio frequency–controlled solid-state relay module; 5—DC power supply; 6—visual interface for power injection and image acquisition control

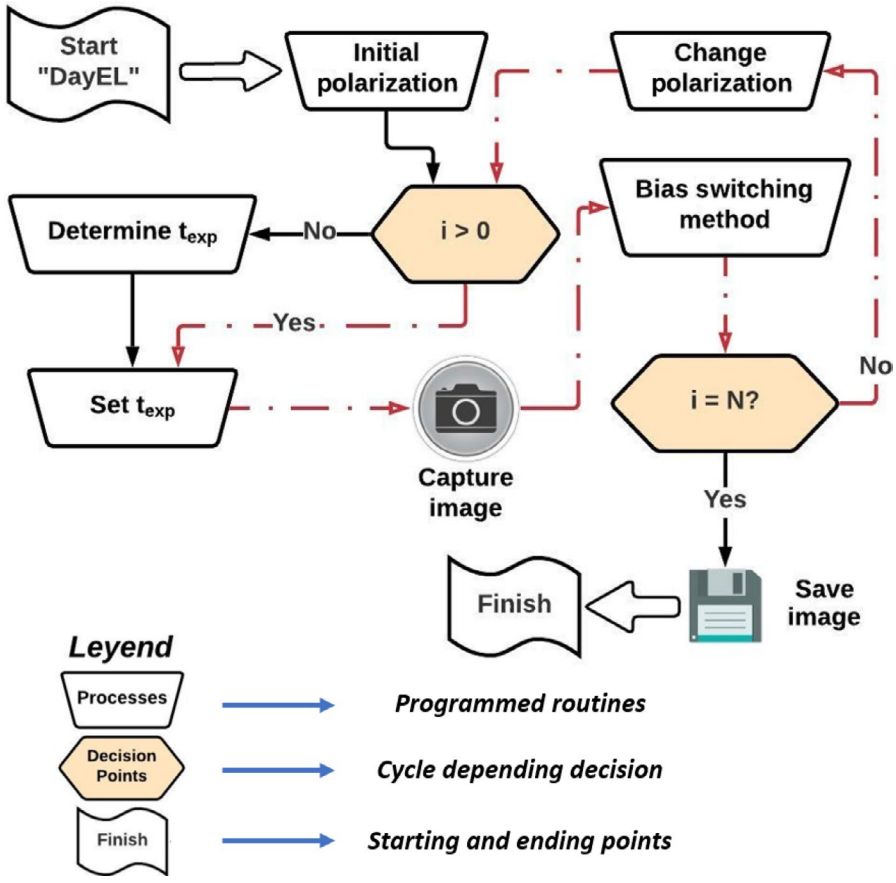

FIGURE 6 Software flow diagram of the "Bias Switching Method"

a solid-state relay was developed (element 4 in Figure 5). Through proprietary software, this element allows the image acquisition and the forward current on the photovoltaic panel to be synchronized.

The procedure for daylight PL measurements is similar. However, because the forward current is not necessary the DC power supply is disconnected. In order to filter the background light, the photovoltaic module must be short-circuited. The radio frequency–controlled solid-state relay module is used for this purpose.

In order to obtain a final EL image, several images (in both On and Off states) must be acquired. One very convenient method for doing this involves acquiring image after image and adding these to the same object (640 × 512 matrix), only accumulating the total sum in the memory. The procedure followed consists of adding the On images and subtracting the Off images, which can be expressed as follows:

$$I_f = \sum_{i=0}^{N} I_{On_i} - I_{Off_i} \quad (2)$$

where N is the total number of cycles in a measurement, I_f is the resulting final image, I_{On_i} represents each image in the On state, and I_{Off_i} represents each image in the Off state.

Figure 6 shows the software flow diagram of the bias switching procedure. The first step is to set the polarization state (On). The software checks the images previously obtained. If there are no previous images ($i = 0$ in Equation 2), the exposure time will be determined by an optimized algorithm and then applied to the subsequent measurements. Then ($i > 0$ in Equation 2), the software will only change the polarization state to obtain the desired images at each time; t_{exp} remains fixed (circuit of dash-dot red arrows in Figure 6). According to Equation (2), when $i = N$ the process will finish after automatically saving the resulting image. The numerical value for N is fixed at the beginning of the measurement process, depending on the background irradiance conditions.

In order to quantify the quality of the luminescence images, our software is also able to provide in real time the result of the SNR averaged over the N cycles (SNR_{AVG}) as proposed in Ref. [45] for outdoor measurements. According to IEC standard 60904-13, the minimum acceptable value for SNR in the case of outdoor EL measurement is 5.

The obtained EL and PL images have not been altered; only the contrast has been modified.

4 | RESULTS AND DISCUSSION

4.1 | Comparison of Si and InGaAs sensors

Figure 7 shows the tests performed for a single On/Off cycle, using a Si CCD camera (A, B) and the InGaAs camera (C, D). The figure shows the processed images (as a result of the difference in signals for the On state and the Off state) obtained under very low background lighting conditions (inside the laboratory, G < 100 W/m^2) for increasing sensor exposure times (t_{exp}). In the case of the Si CCD tests, although a slight improvement is noticeable when increasing t_{exp}, the images present very poor contrast with a high noise level. In addition, the exposure time cannot be increased further as the background light saturates the Si detector.

The processed images obtained with the InGaAs camera for increasing exposure times, under similar low background light conditions (Figure 7C,D), show a high noise for very low t_{exp}, although the SNR increases substantially by increasing t_{exp}. Note that the exposure times with the InGaAs detector are reduced by at least one order of magnitude with respect to the exposure times with the Si detector, due to the high sensitivity of the InGaAs camera in the 1000-1300 nm spectral window (compared to the Si-based one). This is crucial for obtaining fast and high-quality daylight EL images using the bias switching method.

4.2 | Measurements at different irradiance levels

Figure 8A,B shows the EL images obtained with a fixed t_{exp} of 25 ms at noon and in the afternoon, as the solar irradiance decreases along the afternoon. The quality of the image, measured with the SNR_{AVG} value, increases substantially as the solar irradiance decreases (from 8.2 to 22.5). This occurs because even for the same EL signal intensity, when the solar irradiance is lower, the SNR improves (see the schematic

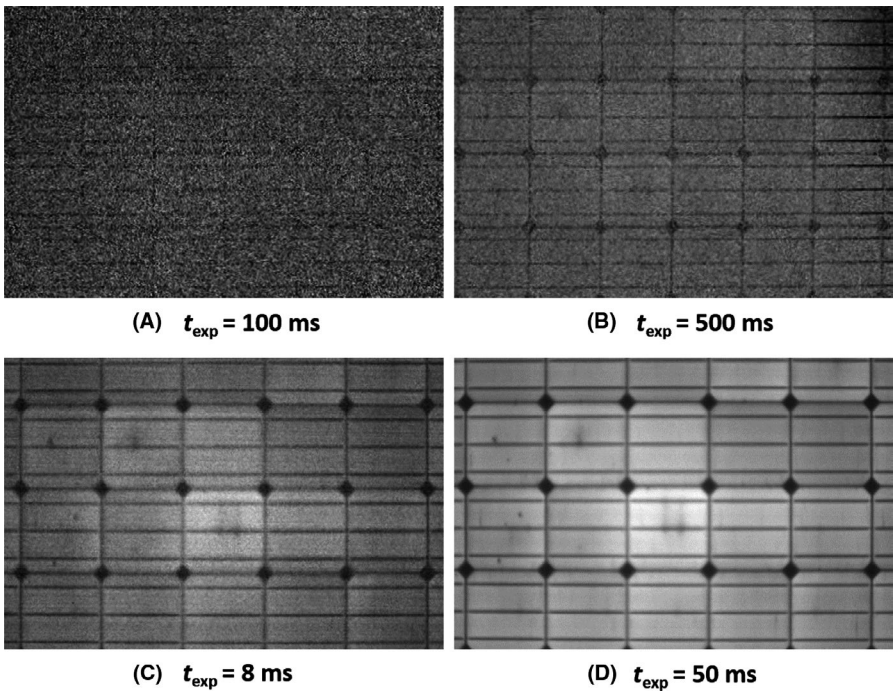

FIGURE 7 Processed EL images (On minus Off) from a monocrystalline Si module obtained with a Si CCD (PCO model) (A, B) and with an InGaAs camera (C, D) under low background irradiance conditions (G < 100 W/m^2) for different exposure times

representation in Figure 3, for high and low irradiance conditions with $t_{exp} = t_1$). Despite this, the EL image obtained under the highest solar irradiance is good enough to clearly detect the defects in the crystalline Si module. Some saturation is observed (blurred areas in the image) which might be associated with fluctuations in solar irradiance or with local changes in panel reflectivity. Under saturation, the difference obtained from subtracting the images would be zero, which can be prevented by adjusting the exposure time.

As solar irradiance decreases, exposure time can be increased in order to improve image quality (see the influence of exposure time (t_2 vs t_1) in the schematic representation of Figure 3). In this case, the SNR is enhanced by increasing the exposure time from 25 ms to 900 ms (Figure 8B,C) (the SNR_{AVG} value increases from 22.5 to 31.4), thereby improving the quality of the image. On the other hand, the increased t_{exp} will lead to an increase in total acquisition time. These two parameters (desired SNR_{AVG} value and total acquisition time) need to be "played with" in order to select the optimum t_{exp}.

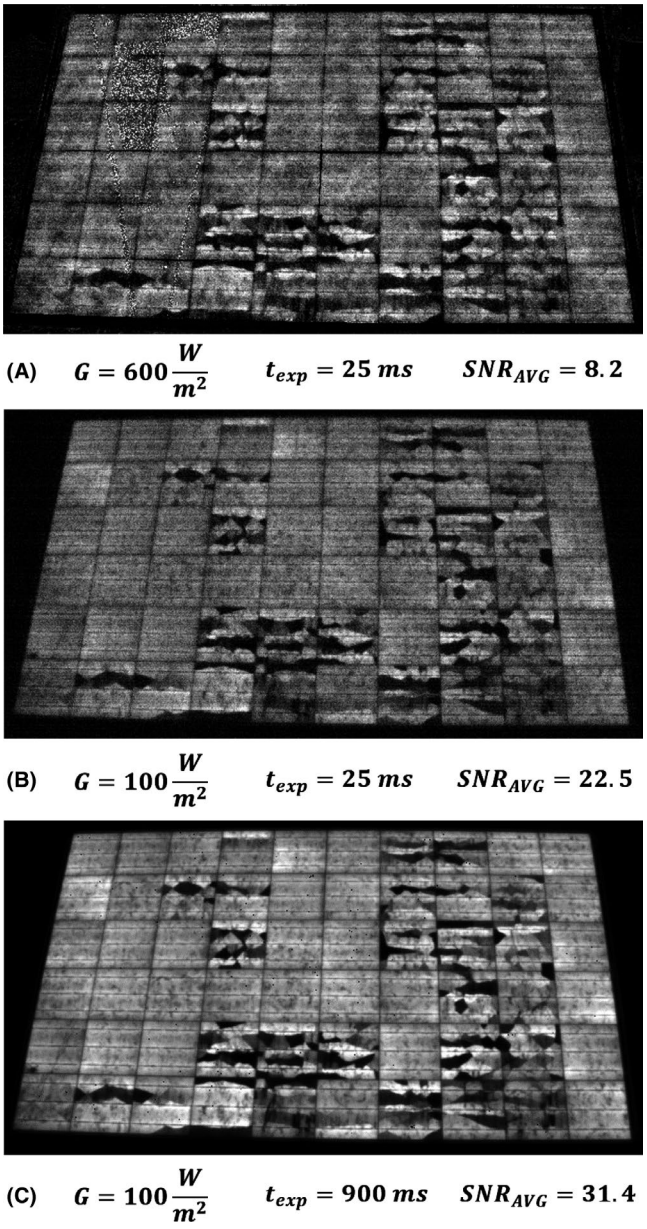

FIGURE 8 EL images for different irradiance conditions (N = 50 cycles). (A) to (B) shows the evolution of the EL image with a fixed exposure time (t_{exp} = 25 ms); (B) to (C) shows the effect of the increment of the exposure time, using the best (highest) exposure time for the lower irradiance case

4.3 | Measurements with different images per cycle

In our quest to improve the SNR, we modified the cycle acquisition by obtaining several consecutive images, rather than only one per cycle and bias state. Figure 9 shows the difference between the images recorded with one, two, and three captures per cycle and bias state. An increase in the SNR_{AVG} value from 5.2 to 8.5 (and thus in the quality of the resulting EL image, which appears better defined) is observed for two image captures, with respect to only one image capture. This is the result of signal averaging. However, when considering the results of capturing more images per cycle, no additional improvement was seen vis-à-vis the situation of two image captures (the SNR_{AVG} value decreases to 7.1 for three captures per cycle). In fact, increasing the number of images per cycle leads to increased acquisition time, yet without any reward in terms of improvement. Moreover, a longer acquisition time is prone to background light variations.

4.4 | Optimal number of cycles and total measurement time

The optimal number of cycles would depend on the solar irradiance level and the desired SNR_{AVG} value. As solar irradiance increases, one would expect to have to increase the number of cycles in order to improve the EL image quality (value of SNR_{AVG}). Several tests with different cycles were performed so as to obtain an estimation of the optimal number of cycles for different levels of solar irradiance. Figure 10 shows the results for irradiances of 230 W/m^2 (A, C, E) and 850 W/m^2 (B, D, F), respectively. In this set of measurements, t_{exp} was fixed at 2 ms. As can be seen, the SNR_{AVG} value increases as a function of the number of cycles. For low irradiance (230 W/m^2), 50 cycles were enough to obtain SNR_{AVG} values above 5 and thus images of sufficient quality (Figure 10C). For an irradiance level of 850 W/m^2, 100 cycles are needed to obtain images with similar SNR_{AVG} values (Figure 10F). The increase in the number of cycles implies an increase in the total time (t_T) required to obtain the final EL image. As already mentioned, these times partially depend

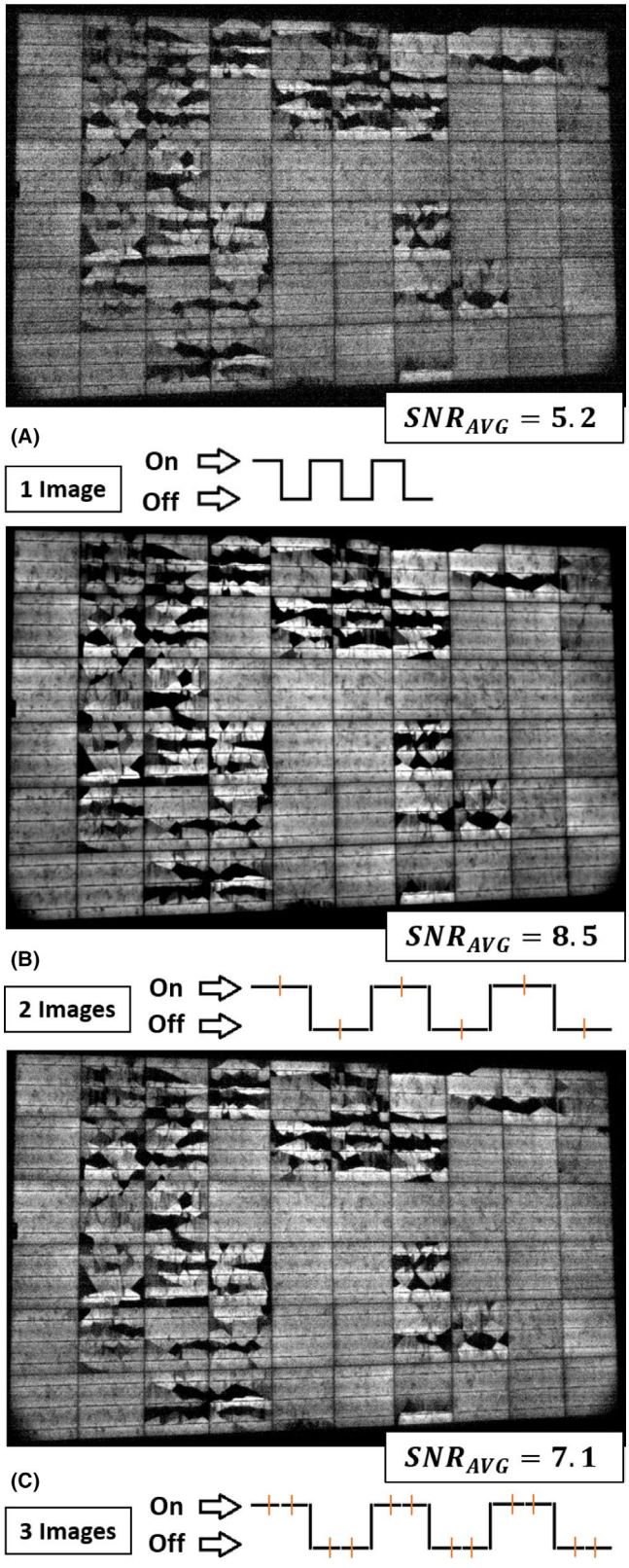

FIGURE 9 Comparison between EL images with 1 (A), 2 (B), And 3 (C) consecutive captures per cycle in each polarization state. $G = 350$ W/m^2, $t_{exp} = 10$ ms, 50 cycles

on the software optimization procedure and on computer capabilities. At present, in our experimental setup with an optimized procedure, 10 cycles would take $t_T = 2.5$ s, while 100 cycles would scale to $t_T = 11$ s. The delay between cycles, combined with a high radiation variation, can occasionally produce a small difference between the images obtained in the two polarization states. The sum of all these small differences may produce a slightly gray backplane in the image.

Although the increase in the number of cycles leads to an increase in the quality of the images (SNR_{AVG} values), the resolution of the InGaAs camera is the main factor that limits the observation of the type and extent of the defects.

4.5 | Polarization of complete strings and individual modules

The resolution of the InGaAs detector would enable EL (PL) images of a complete string of modules to be performed. However, the inclination of the strings and the relative position of the InGaAs detector can greatly affect image quality (because of a lower perpendicular resolution) and, therefore, the ability to distinguish the defects present in each cell. Figure 11 shows EL images of polarized strings with a very large inclination. Some modules are labeled, M1-M4, for comparison with the EL images of those modules taken individually (see Figure 12). These images were obtained under a solar irradiance of 320 W/m^2, an exposure time of 5.5 ms and with 50 cycles. The power supply used in this case was enough to provide more voltage than the sum of the open-circuit voltage of the modules in the string (at least 20% more, such that for a 1000 V string, a 1200 V and a 12 kW power supply would be needed). The trees can be seen in the lower part of Figure 11. Small delays between the images, combined with the movements of mobile parts of the images, produce this effect.

As observed, these EL images provide a preliminary visual observation of degraded modules in the string. However, the classification and identification of the defects are blurred due to low spatial resolution. As the size of the imaged area increases, it becomes increasingly difficult to elucidate the nature of the defects. In fact, depending on the details that one is seeking to image, different resolutions are required.[32,38,46] The EL images of the individual modules labeled in Figure 11 are shown in Figure 12. These daylight EL images are of remarkable quality and enable the defects of the different cells to be identified and classified, which was not possible when imaging the full string, due to the poor spatial resolution (see Figure 11).

4.6 | EL vs PL measurements

EL and PL images of the same module (taken consecutively) under different irradiances (260, 500, and 1140 W/m^2) and

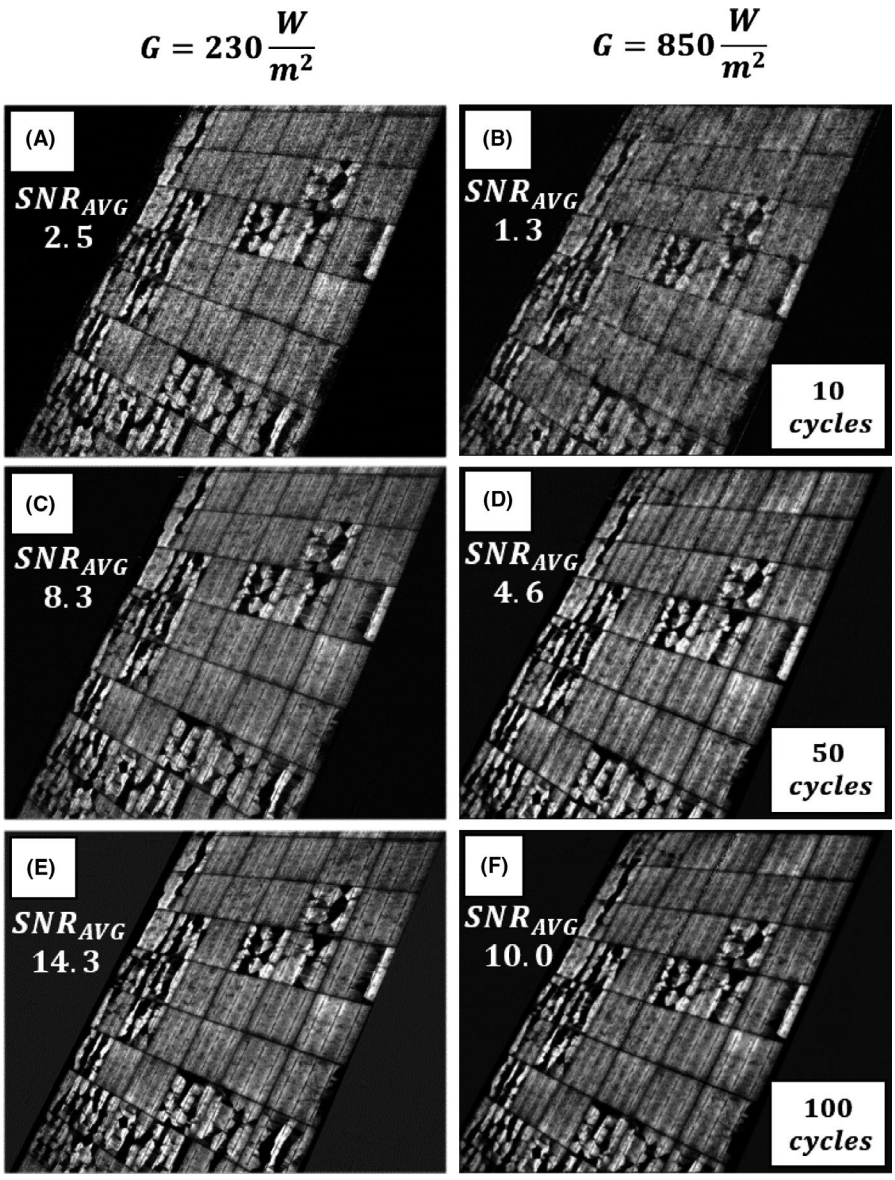

FIGURE 10 EL images obtained with 10 (A, B), 50 (C, D), and 100 (E, F) cycles (t_{exp} = 2 ms in all cases). (A, C, E) 230 W/m^2; (B, D, F) 850 W/m^2

optimized exposure times are shown in Figure 13. The EL images are of high quality for the three irradiances, although the SNR_{AVG} value decreases with irradiance intensity. Instead of this, the PL images improve with irradiance intensity. For low irradiance (260 W/m^2), the PL image is not defined and the main defects are not revealed. For increasing irradiance, the PL images reveal the defect areas, which appear localized in zones of the module for which cracks are observed in the EL images (see the highlighted zones in the EL and PL images [Figure 13C,F]). Nevertheless, there is no one-to-one correlation between PL and EL images, which evidences the complementarity of the two techniques.

Figure 14 shows higher resolution EL (A) and PL (B) images obtained at 980 W/m^2 on the same module, allowing a more detailed visual comparison of the defective areas in the two images. A greater contrast can be seen in the EL images compared to the PL images, which is consistent with the previous discussion, although the PL images are of good quality. One can also clearly distinguish regions where the EL and PL image contrasts are different. Luminescence contrast is governed by the presence of nonradiative recombination centers, electrical fault connections, and the generated e-h population. As formerly mentioned, PL images mainly address the defects associated with cell material, surface passivation, and reflectivity. However, the PL images presented here are not conventional PL images, but need the subtraction of the Off state image, which is also influenced by the contacts. Analysis of the differences between EL and PL images must thus be handled with care. In EL, the carrier population is supplied by current injection, whereas in PL we are dealing with photogenerated carriers. In particular, in Figure 14 the dark contrasted defects are associated with cracks, in which carrier injection is reduced because of the local increase in series resistance, R_s, plus the corresponding contribution of the nonradiative

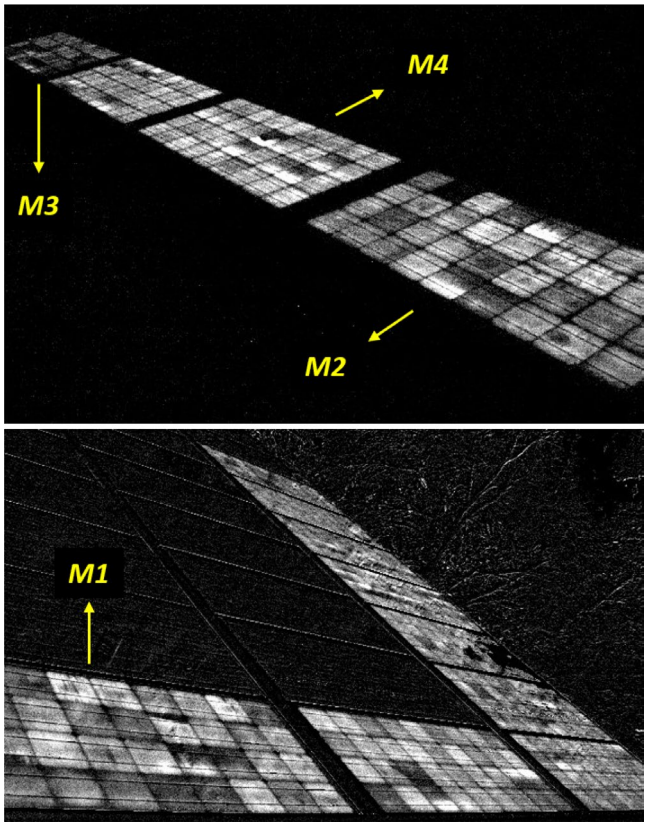

FIGURE 11 EL images of completely polarized strings. $G = 320$ W/m^2, $t_{exp} = 5.5$ ms, 50 cycles. Four modules, labeled M1-M4, are marked for identification purposes (see Figure 12)

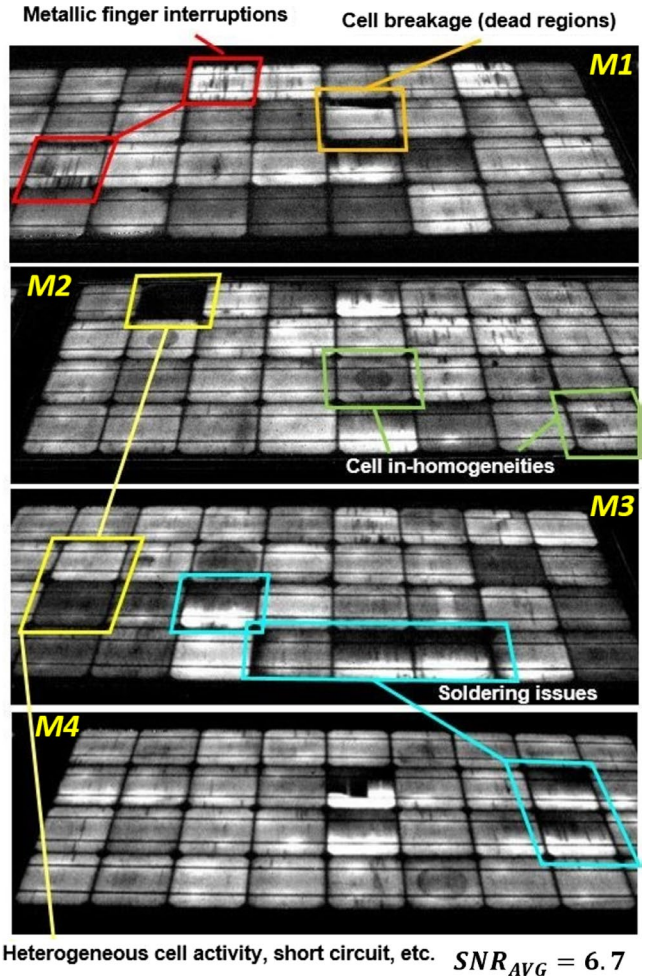

FIGURE 12 EL images of individual modules (labeled M1-M4 in Figure 11), taken independently in a completely polarized string. Easily distinguishable defects are indicated. $G = 320$ W/m^2, $t_{exp} = 5.5$ ms, 50 cycles

recombination. The PL images show local coincidences in the dark contrast with the EL images, although there are other regions with reversed contrast, which is dark in the EL images and bright in the PL images. Additionally, in the PL image the crack boundaries are revealed, giving a dark contrast, which is due to the nonradiative recombination at the crack boundaries. In both measurements, series resistance is relevant, in the On state of EL associated with the injection of carriers and in the Off state of PL associated with the extraction of carriers. Differences in the contrast between EL and PL might therefore be related to the local R_s. The dark contrast in the PL image might be associated with very high local R_s, which does not allow the carriers to be extracted in the PL Off state. It is important to note that a PL signal will also come from an area which is not in electrical contact with the rest of a cell. However, because a difference method is applied here, these areas of the cell will not be in short circuit, such that the difference method will result in a zero signal and thereby give a dark contrast. In those areas, the carrier injection is blocked under direct bias, such that they will also present a dark contrast in the EL images. When isolation is not so high (lower R_s), the extraction of the photogenerated carriers can be sufficient to provide a background image that can be subtracted from the PL image (On state). However, it can produce a sufficient block of the carrier injection to result in the drastic reduction of the EL SNR, therefore giving a dark contrast in the EL image. A quantitative analysis of contrast in these images would provide additional insights into the differences between daylight EL and PL images. Such an analysis lies outside the scope of this paper, but will be the subject of a forthcoming work.

A comparison between EL and PL images of a monocrystalline Si module obtained under the same solar irradiance conditions is shown in Figure 15. Measurements were performed at a very high irradiance level of 1050 W/m^2, corresponding to the city of Madrid at 13:00 on a July day. Both measurements were performed consecutively. Even under such high irradiance levels, the quality of the images is very satisfactory, even for only 50 cycles ($t_T = 7$ s). In these high irradiance conditions, the PL images are very suitable for panel imaging, as seen in the

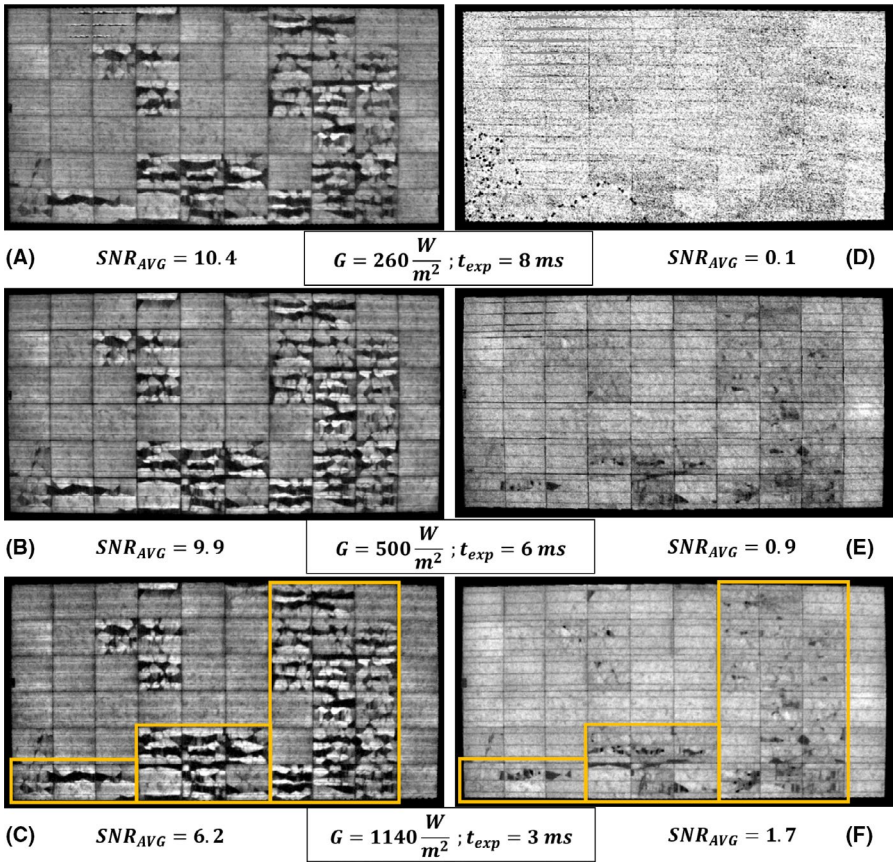

FIGURE 13 Comparison between daylight EL (A-C) and PL (D-F) images obtained consecutively. Irradiance varies from 260 W/m^2 to 1140 W/m^2. The number of cycles was fixed at 50, while t_{exp} was optimized for each case

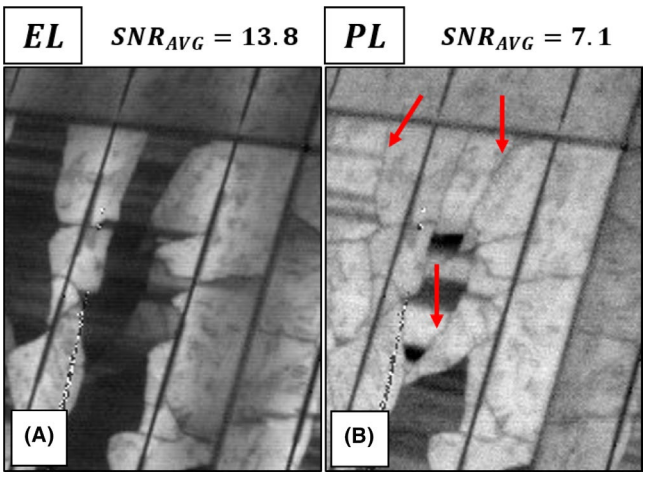

FIGURE 14 Comparison between daylight EL (A) and PL (B) obtained consecutively (close-up view of the same module imaged in Figure 13). G = 980 W/m^2, t_{exp} = 1.9 s, 50 cycles (t_T = 7 s). The arrows indicate crack boundaries

clear daylight PL images (Figure 15B). Despite the high quality of the two images, EL images usually appear more contrasted (SNR_{AVG} = 12.3 for the EL image, compared to SNR_{AVG} = 8.2 for the PL one), revealing more defined details. However, PL images can also reach high quality, and the measurement process is simpler because it does not need the use of a power supply to bias the modules.

4.7 | Very high throughput

The number of Si solar modules that can be measured by using our EL/PL system in a working day can be very high, provided that:

1. complete strings are polarized, and
2. there is a device available to move the InGaAs camera from one module to another rapidly.

Considering the total time required to obtain an image (t_T) and the implementation of remotely controlled relays to switch the strings On and Off, inspection can be done very quickly, reaching throughputs up to 1 MWp/24 h using only one camera and two operators. This is a conservative projection: considering only image acquisition time, around four hours would be required for 1 MW testing. Our EL/PL system appears as a very useful tool for routine inspection of medium- to large-scale photovoltaic plants.[42]

It is important to note that images must be perfectly aligned in our method to ensure that pixel subtraction is occurring for the same physical point on the module. For instance, for aerial use of our method, it is important to ensure the correct subtraction of the images. This is not easy, since it would involve computing time, which is critical in the case of a drone inspection. Aerial luminescence inspections are, nevertheless, beginning to emerge.[5,40]

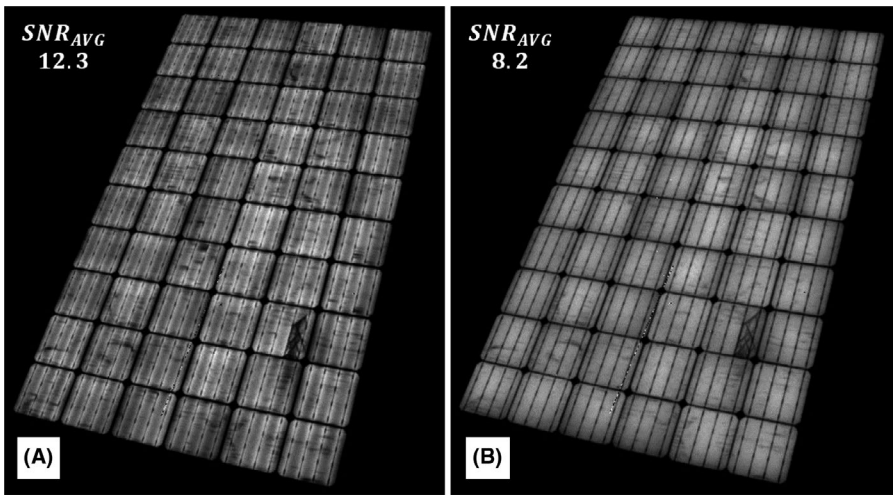

FIGURE 15 Comparison between daylight EL (A) and PL (B) for a monocrystalline Si module, obtained consecutively. $G = 1050$ W/m^2, $t_{exp} = 1.9$ s, 50 cycles ($t_T = 7$ s)

5 | CONCLUSIONS

We implement a user-friendly and cost-effective system capable of acquiring high-quality luminescence (EL or PL) images of Si photovoltaic modules, under the most varied irradiance conditions that can occur in solar plants, 24 hours a day, 365 days a year, and at any latitude. To achieve this, an image processing method was implemented, capable of extracting the luminescence signal in a noisy environment. A bias switching method which makes use of a variable number of On-Off cycles was set up, subtracting the images and averaging them over an optimized number of cycles. The main elements of the system are an InGaAs camera, a band-pass optical filter, a power supply (in the case of EL measurements), and a solid-state relay system for switching from On to Off states. The control and acquisition software was built in LabVIEW. Precise control of the polarization state and synchronized acquisition of the corresponding images, as well as the selection of an optimized exposure time, are fundamental tools of the software package. In order to minimize the problems caused by cable interconnections, a remote control device has been developed to polarize the modules, which allows for switching between the two polarization states, regardless of the power supply used. In order to test the system, inspections of PV modules were carried out in photovoltaic plants, and high-quality images were obtained, which enabled the typical defects found in solar cells, such as microcracks, soldering defects, inhomogeneities, and others, to be detected.

ACKNOWLEDGMENTS

This work was partially financed by Spanish Ministry of Science and Innovation's Industrial Technology Development Center (CDTI), under project IDI-20151194; the Spanish Ministry of Economy, under projects ENE2014-56069-C4-4-R, ENE2017-89561-C4-3-R, and RTC-2017-6712-3; and the Regional Government of Castilla y León, under projects VA081U16 and VA283P18.

ORCID

Miguel Guada https://orcid.org/0000-0003-3412-1700
Ángel Moretón https://orcid.org/0000-0001-5275-8233
Sofía Rodríguez-Conde https://orcid.org/0000-0003-4442-5492
Luis Alberto Sánchez https://orcid.org/0000-0001-8426-1731
Mario Martínez https://orcid.org/0000-0002-1552-0231
Miguel Ángel González https://orcid.org/0000-0001-9130-7339
Juan Jiménez https://orcid.org/0000-0001-6079-332X
Leonardo Pérez https://orcid.org/0000-0001-8028-3968
Vicente Parra https://orcid.org/0000-0001-9201-6656
Oscar Martínez https://orcid.org/0000-0002-2283-0350

REFERENCES

1. Coello J. Introducing electroluminescence technique in the quality control of large PV plants. 26th Eur. Photovolt. Sol. Energy Conf. Exhib. 2013;3469-3472.
2. Bothe K, Pohl P, Schmidt J, et al. Electroluminescence imaging as an in-line characterisation tool for solar cell production. In: *21st Eur. Photovolt. Sol. Energy Conf., Dresden, Germany*; 2006: 597-600.
3. Navarrete M, Pérez L, Domínguez F, et al. On-site inspection of PV modules using an internationally accredited PV mobile lab: a three-year experience operating worldwide. In 31st Eur. Photovolt. Sol. Energy Conf. Exhib. 2015;1989-1991. https://doi.org/10.4229/EUPVSEC20152015-5AV.6.19
4. Koch S, Weber T, Sobottka C, Fladung A, Clemens P, Berghold J. Outdoor electroluminescence imaging of crystalline photovoltaic modules: comparative study between manual ground-level inspections and drone-based aerial surveys. 32nd Eur. Photovolt. Sol. Energy Conf. Exhib. 2016; 1736-1740. https://doi.org/10.4229/EUPVSEC20162016-5DO.12.2

5. dos Reis Benatto GA, Riedel N, Thorsteinsson S, et al. Development of outdoor luminescence imaging for drone-based PV array inspection. *Proc IEEE Int Conf Comput Vis*. 2009;2682-2687.
6. Madeti SR, Singh SN. A comprehensive study on different types of faults and detection techniques for solar photovoltaic system. *Sol Energy*. 2017;158:161-185.
7. Jahn U, Herz M, Köntges M, et al. Review on infrared and electroluminescence imaging for PV field applications. Int Energy Agency Rep IEA-PVPS T13-10; 2018.
8. Rau U. Superposition and reciprocity in the electroluminescence and photoluminescence of solar cells. *IEEE J Photovoltaics*. 2012;2:169-172.
9. Rau U. Reciprocity relation between photovoltaic quantum efficiency and electroluminescent emission of solar cells. *Phys Rev B*. 2007;76(8):1-8.
10. Fuyuki T, Kondo H, Yamazaki T, Takahashi Y, Uraoka Y. Photographic surveying of minority carrier diffusion length in polycrystalline silicon solar cells by electroluminescence. *Appl Phys Lett*. 2005;86:1-3.
11. Spataru S, Parikh H, Hacke P, dos Reis Benatto GA, Sera D, Poulsen PB. Quantification of solar cell failure signatures based on statistical analysis of electroluminescence images. In: *Proc. 33rd Eur. Photovolt. Sol. Energy Conf. Exhib.*, 2017;1466-1472.
12. Köntges M, Kurtz S, Packard CE, et al. Review of Failures of Photovoltaic Modules. 2014. https://iea-pvps.org/wp-content/uploads/2020/01/IEA-PVPS_T13-01_2014_Review_of_Failures_of_Photovoltaic_Modules_Final.pdf
13. Fruehauf F, Turek M. Quantification of electroluminescence measurements on modules. *Energy Procedia*. 2015;77:63-68.
14. Jordan DC, Silverman TJ, Wohlgemuth JH, Kurtz SR, VanSant KT. Photovoltaic failure and degradation modes. *Prog Photovoltaics Res Appl*. 2017;25(4):318-326.
15. Höffler H, Haunschild J, Rein S. Influence of external contacting on electroluminescence and fill factor measurements. *Sol Energy Mater Sol Cells*. 2016;152:180-186.
16. Potthoff T, Bothe K, Eitner U, Hinken D, Königes M. Detection of the voltage distribution in photovoltaic modules by electroluminescence imaging. *Prog Photovoltaics Res Appl*. 2010;18:100-106.
17. Tsai DM, Wu SC, Li WC. Defect detection of solar cells in electroluminescence images using Fourier image reconstruction. *Sol Energy Mater Sol Cells*. 2012;99:250-262.
18. Parikh H, Spataru S, Sera D, et al.Enhancement of Electroluminescence images for fault detection in photovoltaic panels. In: Proc. IEEE 7th WCPEC. 2018; 447-452. https://doi.org/10.1109/PVSC.2018.8547442
19. Bhoopathy R, Kunz O, Juhl M, Trupke T, Hameiri Z. Outdoor photoluminescence imaging of photovoltaic modules with sunlight excitation. *Prog Photovoltaics Res Appl*. 2018;26(1):69-73.
20. Stoicescu L, Gedeon P, Gläser GC. Full area simulation of multicrystalline silicon solar cells with high spatial resolution. In: Conf. Rec. IEEE Photovolt. Spec. Conf. 2011. https://doi.org/10.1109/PVSC.2011.6186701
21. Trupke T, Mitchell B, Weber JW, McMillan W, Bardos RA, Kroeze R. Photoluminescence imaging for photovoltaic applications. *Energy Procedia*. 2012;15:135-146.
22. Demant M, Haunschild J, Nievendick J, et al. Quality control of as-cut multicrystalline silicon wafers using photoluminescence imaging for solar cell production. *Sol Energy Mater Sol Cells*. 2010;94:2007-2012.
23. Shen C, Wang K, Green MA. Fast separation of front and bulk defects via photoluminescence on silicon solar cells. *Sol Energy Mater Sol Cells*. 2014;128:260-263.
24. Sánchez LA, Moretón A, Guada M, Rodríguez-Conde S, Martínez O, Jiménez J. Defect characterization of UMG mc-Si solar cells using LBIC and luminescence imaging techniques. *MRS Adv*. 2018;3:3359-3365.
25. Moralejo B, Tejero A, Hortelano V, Martínez O, González MA, Jiménez J. Defect recognition by means of light and electron probe techniques for the characterization of mc-Si wafers and solar cells. *Superlattices Microstruct*. 2016;99:45-53.
26. Sánchez LA, Moretón A, Guada M, et al. Photoluminescence imaging and LBIC characterization of defects in mc-Si solar cells. *J Electron Mater*. 2018;47:5077-5082.
27. Guerrero I, Parra V, Carballo T, et al. About the origin of low wafer performance and crystal defect generation on seed-cast growth of industrial mono-like silicon ingots. *Prog Photovolt Res Appl*. 2012;17:115-125.
28. dos Reis Benatto GA, Chi M, Jensen OB, et al. Photoluminescence imaging induced by laser line scan: study for outdoor field inspections. In: 2018 IEEE 7th World Conf. Photovolt. Energy Convers. 2018; 395-399. https://doi.org/10.1109/PVSC.2018.8547416
29. Silverman T, Deceglie M, VanSant K, Johnston S, Repins I. Illuminated outdoor luminescence imaging of photovoltaic modules. In: IEEE 44th PVSC. 2017. https://doi.org/10.1109/PVSC.2017.8366288
30. Walter D, Fell A, Franklin E, MacDonald D, Mitchell B, Trupke T. The impact of silicon CCD photon spread on quantitative analyses of luminescence images. *IEEE J Photovoltaics*. 2014;4:368-373.
31. Mertens K, Arnds A, Behrens G, Dominik A. Low-cost-outdoor-electroluminescence: significant improvements of the method. In: 32nd EUPVSEC. 2016; 2081-2083. https://doi.org/10.4229/EUPVSEC20162016-5BV.2.75.
32. Frazao M, Silva JA, Lobato K, Serra JM. Electroluminescence of silicon solar cells using a consumer grade digital camera. *Measurement*. 2017;99:7-12.
33. Pérez L, Coello J, Domínguez F, Navarrete M.Development and implementation of a Mobile Laboratory - PV MOBILE LAB Quality assurance of photovoltaic modules “On Site”. In: 28th Eur. Photovolt. Sol. Energy Conf. Exhib., n.d.: 3500-3504.
34. Adams J, Doll B, Buerhop C, et al. Non-Stationary Outdoor EL-measurements with a fast and highly sensitive InGaAs Camera. 32nd Eur. Photovolt. Sol. Energy Conf. Exhib. 2015;1837-1841.
35. Köntges M, Kajari-Schröder S, Kunze I, Jahn U. Crack statistic of crystalline silicon photovoltaic modules. In: 26th Eur. Photovolt. Sol. Energy Conf. Exhib. 2014;3290-3294.
36. Munoz MA, Alonso-García MC, Vela N, Chenlo F. Early degradation of silicon PV modules and guaranty conditions. *Sol Energy*. 2011;85:2264-2274.
37. Kropp T, Berner M, Stoicescu L, Werner JH. Self-sourced daylight electroluminescence from photovoltaic modules. *IEEE J Photovoltaics*. 2017;7:1184-1189. https://doi.org/10.1109/JPHOTOV.2017.2714188
38. Stoicescu L, Reuter M, Werner JH.DaySy: luminescence imaging of PV modules in daylight. In: 29th Eur. Photovolt. Sol. Energy Conf. Exhib. (n.d.) 2553-2554.
39. Stoicescu LM, Reuter M, Werner JH. Method and apparatus for testing photovoltaic modules US patent. US9680412B2. 2017.

40. dos Reis Benatto GA, Riedel N, Mantel C, et al. Luminescence imaging strategies for drone-based PV array inspection. 33rd Eur. Photovolt. Sol. Energy Conf. Exhib. 2017.
41. Parikh H, Spataru S, Séra D, et al. A photovoltaic module diagnostic setup for lock-in electroluminescence imaging. In: 46th IEEE PVSC. 2019.
42. Martínez O, Guada M, Moretón Á, et al. Implementation of a friendly daylight electroluminescence system for the inspection of solar PV panels. In: 34th Eur. Photovolt. Sol. Energy Conf. Exhib. 2017;2021-2025.
43. Breitenstein O, Langenkamp M. *Lock-in Thermography*. Berlin: Springer; 2001.
44. Bedrich KG, Bliss M, Betts TR, Gottschalg R. Electroluminescence imaging of PV devices: camera calibration and image correction. In: 43th IEEE PVSC. 2016;1532-1537. https://doi.org/10.1109/PVSC.2016.7749875
45. Mantel C, dos Reis Benatto GA, Riedel N, et al. SNR study of outdoor electroluminescence images under high sun irradiation. In: IEEE 7th World Conf. Photovolt. Energy Convers. 2018. https://doi.org/10.1109/PVSC.2018.8548264
46. Silva JA, Serra JM, Vallêra AM, Lobato K.Luminescence in Photovoltaics. In: Fluoresc. Ind. Switzerland: Springer Nature, 2019; 173-211. https://doi.org/10.1007/4243_2018_7

How to cite this article: Guada M, Moretón Á, Rodríguez-Conde S, et al. Daylight luminescence system for silicon solar panels based on a bias switching method. *Energy Sci Eng*. 2020;8:3839–3853. https://doi.org/10.1002/ese3.781